JOURNAL OF AIRCRAFT
Vol. 47, No. 3, May–June 2010

# Experimental Investigation of a Circular-Planform Concept Aircraft

Bryan Recktenwald*
*Archangel Systems, Inc., Auburn, Alabama 36832*
and
Gilbert L. Crouse Jr† and Anwar Ahmed‡
*Auburn University, Auburn, Alabama, 36849*

DOI: 10.2514/1.46149

**This paper presents experimental results from wind-tunnel testing of a novel aircraft configuration known as the Geobat. This configuration has a circular planform with the forward portion of the disk serving as the main wing and body of the aircraft, and an aft portion that serves as the horizontal stabilizer. The two parts are attached at the wing tips much like a joined-wing design, and also near the centerline by two booms supporting vertical stabilizers. The center portion of the body is open. Wind-tunnel tests were conducted to determine the lift, drag, and pitching moment characteristics of the configuration. For comparison purposes, two flat disks were also tested, one with a similar interior cutout and one solid across the full disk. Experimental data have been compared with vortex-lattice analysis for the solid and cutout shapes. Comparisons of the theory and experimental data indicate that viscous and vortex lift effects strongly influence the performance of the configuration, particularly at higher angles of attack. Both the experimental data and analysis show that the Geobat planform moves the aerodynamic center slightly aft, and the geometry tends to push the center of gravity forward, improving the static stability versus a solid-disk-shaped wing design.**

## Nomenclature

| | | |
|---|---|---|
| $C_{D_i}$ | = | induced drag coefficient |
| $C_{D_0}$ | = | drag coefficient at zero lift |
| $C_L$ | = | lift coefficient |
| $C_{L_{\max}}$ | = | maximum lift coefficient |
| $C_{L_\alpha}$ | = | lift curve slope, 1/rad |
| $C_{L_{\alpha=0\ \deg}}$ | = | lift coefficient at zero angle of attack |
| $C_{M_{\mathrm{ac}}}$ | = | pitching moment coefficient about the aerodynamic center |
| $e$ | = | span efficiency factor for lift, defined such that $C_{L_\alpha} = \frac{2\pi}{1+\frac{2\pi}{\pi e \mathrm{AR}}}$, or span efficiency factor for drag, defined such that $C_{D_i} = \frac{C_L^2}{\pi e \mathrm{AR}}$ |
| $L/D_{\max}$ | = | maximum value of lift-to-drag ratio |
| $x_{\mathrm{ac}}$ | = | longitudinal location of aerodynamic center, percent chord |
| $\alpha_{L/D_{\max}}$ | = | angle of attack at which lift-to-drag ratio is maximized, deg |
| $\alpha_{L=0}$ | = | angle of attack at which lift is zero, deg |
| $\alpha_{\text{min drag}}$ | = | angle of attack for minimum drag, deg |
| $\alpha_{\text{stall}}$ | = | angle of attack at which lift coefficient is maximized, deg |

## Introduction

DISK-SHAPED flying bodies have been around for thousands of years. The sport of discus throwing was a part of the ancient Olympic Games as early as 708 BC.[§] In recent times, the Frisbee® flying disk is the most widespread example of a circular wing, but a number of engineering studies have also been conducted on flying disks. In the late 1960s the U.S. Navy commissioned a project in which the aerodynamic characteristics of a self-suspended Frisbee-shaped flare were investigated [1]. Both spinning and nonspinning models were tested, and it was found that spin had negligible effects on the aerodynamic forces and moments. Later, Stilley and Carstens [2] analyzed flight stability and compared actual flights to free-fall tests.

For aircraft applications, circular-planform wings can be classified as low aspect ratio (AR) wings. The two broad categories of circular-planform designs are annular wings that have an open center and solid-disk shapes. The first annular wing aircraft to fly was designed and built by Lee-Richards, circa 1911–1914 [3], a replica of which now resides in The Science Museum in London. A solid-disk-shaped airplane, but with a straight leading edge, was first built by Snyder [4], who flew his "Dirigiplane" glider in 1932; this was followed by a powered version called the Arup S-2, which used a NACA M-6 airfoil that gave slightly better performance compared to a Clark-Y airfoil [5]. A perfectly circular disk-shaped aircraft was flown by Johnson in 1931 and patented in 1932 [6]. Both Snyder's and Johnson's designs were later incorporated in the famous "Flying Pancake" of Zimmerman [7], which later flew as the Vought V-173 and its derivative the XF5U-1 [8].

A type of disk-shaped flight vehicle of lenticular configuration (biconvex cross section and circular planform) was investigated as a reentry vehicle because of its high volumetric efficiency compared to a conventional tubular fuselage [9]. Low-speed tests revealed that the lenticular body was longitudinally unstable for low angles of attack but that stability improved at higher angles of attack [10]. However, with the help of external fins and body pylons, higher stability and a better $L/D$ ratio were obtained [11].

In the early 1970s, Kissinger devised and patented a circular-planform design [12] that incorporated a circular wing with a small cutout in the rear portion for a pusher propeller and with a portion of the aft disk raised above the propeller wake to serve as a horizontal stabilizer. The circular wing was mounted above a conventional fuselage. The wing shape was similar to a configuration patented in

Presented as Paper 371 at the 46th AIAA Aerospace Sciences Meeting and Exhibit, Reno, NV, 7–10 January 2008; received 25 June 2009; accepted for publication 18 September 2009. 

*Engineer, 1635 Pumphrey Avenue.
†Associate Professor, Aerospace Engineering Department, 211 Aerospace Engineering Building. Senior Member AIAA.
‡Professor, Aerospace Engineering Department, 211 Aerospace Engineering Building. Associate Fellow AIAA.

§Data available online at http://www.britannica.com/EBchecked/topic/428005/Olympic-Games [retrieved 5 Sept. 2008].

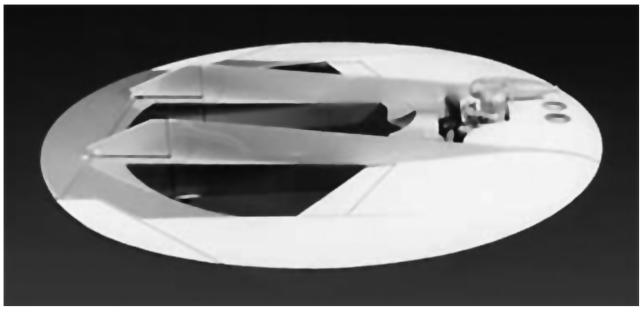

**Fig. 1 Geobat prototype.**

1925 by Myers [13]. However, Myers' design did not include the vertical stabilizers or raised horizontal stabilizer included by Kissinger.

In the last 10 years, several other wind-tunnel tests have been performed on circular disk configurations. Mitchell [14] measured lift and drag on nonspinning disks. Yasuda [15] measured lift and drag for a range of flow speeds and spin rates for Frisbees and flat plates. Potts and Crowther [16] embarked upon many wind-tunnel tests on disk-shaped bodies. They not only measured the lift and drag but also the pitching and rolling moments. Additionally, they analyzed pressure distributions and airflow around the Frisbee and verified the aerodynamic effects of spin measured earlier by Stilley [1]. They found that, although observable, the effects of spin were not overly important in the generation of aerodynamic forces. Ali [17] performed comprehensive measurements of lift, drag, and pitching moment for nonspinning disk–wing configurations and concluded that flat disk configurations posed concerns for longitudinal stability.

In addition to these experimental studies, a number of researchers have studied exact theoretical solutions to the lift force on a circular disk, including Jordan [18], and Tuck and Lazauskas [19]. Jordan [18] developed an analytical approach using a truncated infinite series solution of the potential flow problem. His results for the circular disk gave a lift curve slope of 1.79/rad and the location of the aerodynamic center as 23.95% of the disk chord.

The present research was undertaken to investigate and document the aerodynamic characteristics of the Geobat configuration, a design that was first conceived, built, and flown in the early 1990s by Jack Jones, a radio-controlled model airplane enthusiast [20]. An early prototype is shown in Fig. 1. Reports from informal flight testing indicate excellent low-speed handling qualities, maneuverability, and high-angle-of-attack characteristics. The circular geometry also makes for a very robust structure.

The Geobat design bears some similarity to the design earlier explored by Kissinger [12] and the Panaflight Corporation. However, that design had a relatively small opening in the back of the disk wing for its pusher propeller and should basically be considered a circular-planform wing. In contrast, the Geobat configuration has a substantially larger (50% of the overall planform area) opening in the aft center portion of the disk and, consequently, appears to behave aerodynamically more like a joined-wing aircraft rather than a single monolithic disk wing. Moreover, the Geobat configuration has the fuselage blended into the forward portion of the disk rather than having the wing mounted above a conventional fuselage.

The objective of this investigation has been to develop an experimental database for further aerodynamic improvements and computational modeling. To support this goal, a series of wind-tunnel tests were conducted in the Auburn University $1 \times 1.2$ m closed-circuit wind tunnel. These tests included two variations of the Geobat configuration (one with a transition strip on the leading edge and one with a clean surface) and two flat plate models (one a solid disk and one with the same internal cutouts as the Geobat model).

## Experimental Setup

### Model Geometry

The Geobat model tested had a disk-shaped body with a 56 cm outer diameter and a central opening. The model can be best described as a joined wing with a circular arc backswept front wing and straight trailing edge, and a forward-swept rear wing with a circular trailing edge. Both wings were joined at the tips, thus creating a 360 deg circular planform. The control surfaces included front and rear ailerons, a large elevator, and two rudders. Each section of the Geobat model was contoured with a NACA 23012 series airfoil geometry. Figure 2 shows a top schematic view of the Geobat model.

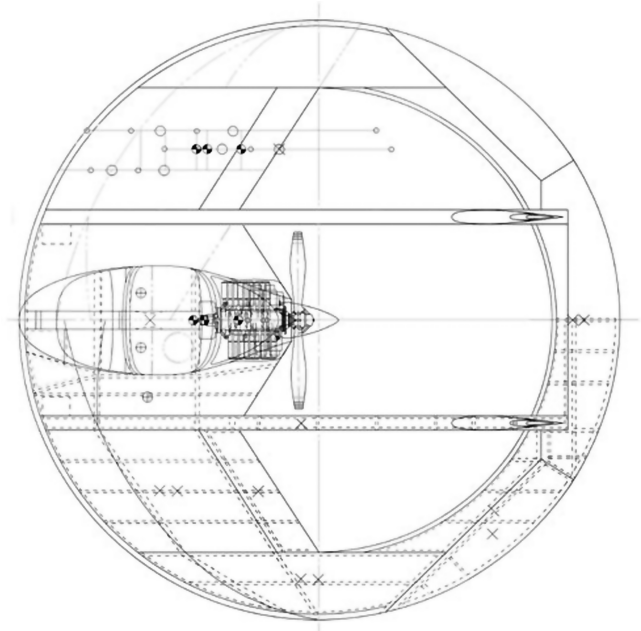

**Fig. 2 Schematic of the Geobat model airplane.**

Two full series of tests were performed on the Geobat model. During the first series, the model surface was left smooth. For the second series, a transition strip consisting of 120-grit pumice was attached to the front 10% of the airfoil on both the upper and lower surfaces to ensure a fully turbulent boundary layer in the flow over the model. The transition strip is visible in Fig. 3.

### Disk Geometry

Two flat disks with a 56 cm diameter made from 5-mm-thick aluminum stock were also tested. Both disks had their edges beveled at 45 deg and were mounted at their respective centers of mass. One of the disks was solid and the other had an interior cutout shape similar to the Geobat model. The goal of these models was to investigate thickness effects for comparison purposes. Figure 4 shows drawings of the two disk models used.

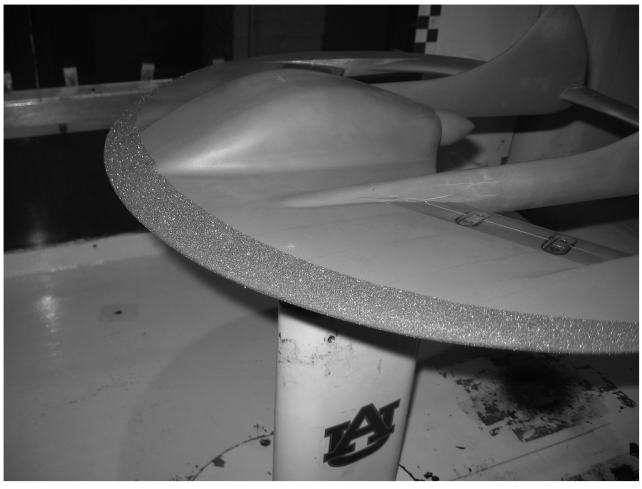

**Fig. 3 Geobat model with transition strip installed in the wind tunnel.**

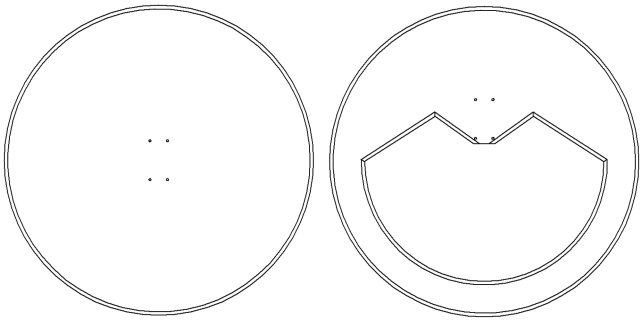

**Fig. 4 Schematics of flat disk models.**

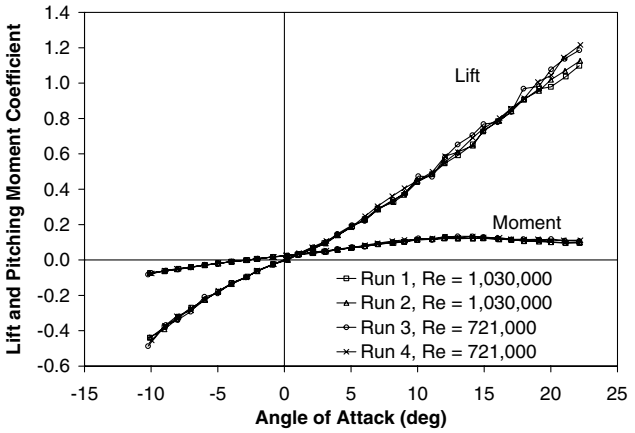


**Fig. 5 Measurement repeatability.**

### Test Setup

Experiments were conducted in the Auburn University $1 \times 1.2$ m, low-subsonic, closed-circuit wind tunnel with speeds capable of 55 m/s. Force and moment data were acquired using a six-component, strain-gauge-type pyramidal balance. Signal conditioning was accomplished with the help of Analog Devices instrumentation amplifiers and National Instruments 16-bit A/D converters. Labview data acquisition software was used to acquire data at a 500 HZ sampling frequency. For each angle of attack setting, 2 s of data (1000 samples) was acquired after a 10 s settling time. These raw data samples were averaged using a Labview program and stored in coefficient form. For each model, data were acquired over an angle-of-attack range from −5 to 20 deg in 1 deg increments. Weight tares were collected at each angle-of-attack setting before starting each tunnel run. Calibration checks of the pyramidal balance were performed before each test series using known weights, and uncertainty analyses of these data showed a maximum error of 2%. Before model testing, the flow angularity of the tunnel was measured and found to be less than 2 deg in the horizontal plane [21].

The measurement repeatability is shown in Fig. 5 for four different runs at two Reynolds numbers for the solid disk. In the linear region, the intervals between the data points are quite small, indicating good repeatability. At very high angles of attack, some differences between the two Reynolds numbers become apparent, as would be expected.

**Table 1 Model parameters and test conditions**

| | Geobat | Solid disk | Cutout disk |
|---|---|---|---|
| Reference area | 0.122 $m^2$ | 0.245 $m^2$ | 0.122 $m^2$ |
| Reference chord | 25 cm | 56 cm | 25 cm |
| Moment reference location (aft of leading edge) | 17 cm | 25 cm | 17 cm |
| Airfoil section | 23,012 | Flat plate | Flat plate |
| Reynolds number | 447,000 | 1,008,000 | 447,000 |

Table 1 presents the parameters associated with each of the three models that were tested and the test conditions. Because all cases were run at the same speed, 30 m/s, the solid disk has the highest Reynolds number due to its larger chord length. The unit Reynolds number for the tests was 550,000.

In addition to the force and moment data acquired and presented here, surface flow visualization tests were also conducted using powdered yellow fluorescent dye mixed in engine oil and a small quantity of oleic acid. The mixture was brushed onto the model surface and the tunnel was quickly brought to the operating condition. Once the flow was established, photographic records were made using an ultraviolet strobe light for illumination. These data are available in [21].

## Vortex-Lattice Analysis

To assist in evaluating the experimental results, a vortex-lattice technique was used to analyze the flow over both the circular disk geometry and the cutout disk geometry. The vortex-lattice method models potential flow over a surface through the use of a collection of horseshoe vortices distributed over the surface in a lattice arrangement (e.g., Katz and Plotkin [22]). In this method, the strength of each of the vortex segments is calculated by setting up a system of equations to enforce flow tangency to the surface. Once the strength of each of the vortex segments in known, the lift, moment, and induced drag over the surface can be calculated. The software program Athena Vortex Lattice (AVL) by Drela and Youngren [23] implements this type of methodology and was used for this study.[¶] Representations of the circular disk and the cutout disk were created using the software and are illustrated in Figs. 6 and 7.

Using the AVL program, lift curve slopes and aerodynamic center calculations were performed and the results are shown in Table 2.

To evaluate the accuracy of the vortex-lattice solutions, the results for the solid disk were compared with the theoretical values from Jordan [18]. Excellent agreement was achieved for both the lift curve slope (0.05% difference) and aerodynamic center estimate (0.01% difference). This provides some confidence in the accuracy of the vortex-lattice results.

Using these analytical results to compare the aerodynamic performance of the solid disk to the cutout disk is made more complicated by the differences in the aspect ratio and reference area between the two. To allow direct comparison, the lift curve slope was examined in terms of span efficiency, $e$. From finite wing theory [24], the three-dimensional lift curve slope of a wing, $C_{L_\alpha}$, can be written as follows:

$$C_{L_\alpha} = \frac{2\pi}{1 + \frac{2\pi}{\pi e \mathrm{AR}}}$$

assuming a 2-D lift curve slope, $C_{l_\alpha} = 2\pi$. For an ideal wing with an elliptical lift distribution, $e$ would be 1. This equation can be solved for span efficiency in terms of the three-dimensional lift curve slope, $C_{L_\alpha}$, to yield

$$e = \frac{2}{\mathrm{AR}}\left(\frac{C_{L_\alpha}}{2\pi - C_{L_\alpha}}\right)$$

Although finite wing theory is not strictly applicable to such low aspect ratio surfaces, the comparison of the two span efficiency values provides some insight into the relative performance of the two planforms. Table 3 presents the calculated span efficiencies. Because the span efficiency for the cutout disk (75%) is considerably higher than that for the solid disk (63%), it indicates that removing the area for the cutout disk has improved the lift generating capabilities of the planform beyond the improvement from just the increase in aspect ratio.

The lift-to-induced-drag ratio of the two planforms is presented in Table 2 at a lift coefficient of $C_L = 0.3$. The cutout disk has a much

[¶]Data available online at http://web.mit.edu/drela/Public/web/avl/ [retrieved 22 Oct. 2007].

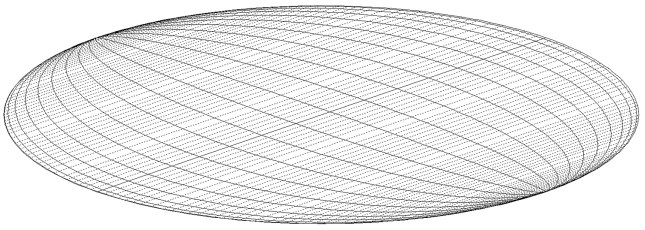

**Fig. 6 Vortex-lattice representation of flat disk.**

higher $L/D$ by a factor of over two at that specific lift coefficient. However, this is somewhat misleading because the two planforms have different areas; consequently, a lift coefficient of 0.3 for the solid disk corresponds to a lift coefficient of 0.6 for the cutout disk. To allow a more fair comparison, the span efficiency concept will be used again as it was for the lift curve slope. Finite wing theory [24] provides an equation for induced drag of the form

$$C_{D_i} = \frac{C_L^2}{\pi e \mathrm{AR}}$$

which can then be solved for span efficiency to yield

$$e = \frac{C_L^2}{\pi C_{D_i} \mathrm{AR}}$$

Given the induced drag coefficient and lift coefficient computed from the vortex-lattice analysis, this equation can be used to calculate the span efficiency. Comparing the computed span efficiency rather than the induced drag coefficient removes the effect of the difference in reference area between the two planforms and allows direct comparison of their relative drag efficiency. Results for the solid disk and cutout disk are presented in Table 3. Both span efficiencies for induced drag were essentially equal to one, which indicates that both planforms achieved elliptical lift distributions. This is unsurprising for the solid disk because a circular shape is a special case of an ellipse, but it is interesting that the cutout disk also achieves an elliptical distribution and is thus an efficient shape from an induced drag standpoint. That the span efficiency for the cutout disk is greater than one probably indicates some numerical inaccuracy in the vortex-lattice solution rather than an actual improvement over the solid disk.

The final parameter examined using the vortex-lattice method was the aerodynamic center. The aerodynamic center location for a wing is typically located very near a point one-quarter of the chord length aft of the leading edge. For a circular wing this is problematic because the center of volume and, hence, the center of gravity if the weight is evenly distributed is at the midchord position; thus, the center of gravity will be behind the aerodynamic center. This results in a statically unstable configuration. The vortex-lattice code predicts an aerodynamic center location for the solid disk just in front of 24% of the chord. For the cutout disk, the vortex-lattice code predicts an aerodynamic center just behind 25% chord. This is not a substantial movement, but does indicate that removing area from the disk slightly improves the static stability of the wing by moving the aerodynamic center aft. Note, however, that the vortex-lattice analysis is a potential flow analysis and, as such, does not include the effects of viscosity in the flow. For example, it is anticipated that the wake from the forward portion of the disk will affect the flow over the aft portion of the disk. Most likely, this would tend to move the aerodynamic center closer to that of the solid disk, but a potential flow analysis does not capture this type of effect.

**Table 2 Vortex-lattice solutions for lift, drag, and moment**

| | Solid disk | Cutout disk |
|---|---|---|
| Lift curve slope | 1.7909 1/rad | 3.0630 1/rad |
| Aerodynamic center | 23.96% chord | 25.13% chord |
| $L/D_i$ at $C_L = 0.3$ | 13.8 | 29.4 |

**Table 3 Span efficiencies inferred from vortex-lattice analysis**

| | Solid disk | Cutout disk |
|---|---|---|
| Span efficiency, lift curve slope | 63% | 75% |
| Span efficiency, induced drag | 100% | 102% |

## Experimental Results and Discussion

The measured force and moment data that are presented in this section were all acquired at a freestream velocity of 30 m/s. To assist in evaluating and understanding these experimental results, they are presented alongside the experimental data on solid disks collected by Potts and Crowther [16], the theoretical data on solid disks from Jordan [18], and the vortex-lattice analytical data presented in the previous section.

Figures 8 and 9 show the lift and pitching moment for the solid disk in comparison to both the theoretical solution and the test data from Potts and Crowther [16]. The lift curve comparison between the two sets of test data is excellent. Comparison with the theoretical solution is quite good also, particularly at low angles of attack. As the angle of attack increases above several degrees, the test data show an increase in lift curve slope that can be attributed to vortex lift [25]. Note that the vortex-lattice data were not presented for the solid disk because they would overlay the theoretical solution data. The pitching moment comparison between the Potts and Crowther data and the theoretical solution is also very good in the linear range. Although the slopes of all three curves are consistent at low angles of attack, the moment data from the present research show a fairly pronounced shift upward and to the left. This same shift will be seen in the data for all four of the models tested. Because the model is symmetric top and bottom except for the edge bevel, this zero-angle-of-attack moment offset can be attributed to interference caused by the model support and its fairing. The moment curve slopes measured in the present research and those measured by Potts and Crowther match fairly well, as does the location (i.e., the lift coefficient) where the break in the moment curve occurs. However, the two curves do diverge above the break. The Potts and Crowther data show a more stable (nose-down) break than is displayed in the data from this study. This is not

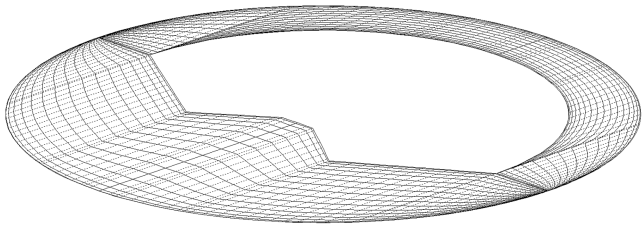

**Fig. 7 Vortex-lattice representation of cutout disk.**

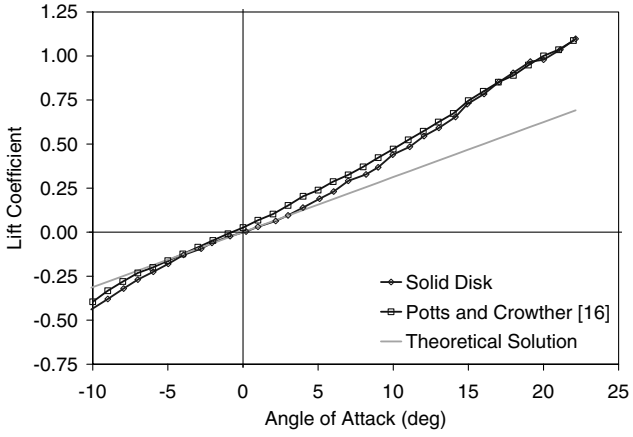


**Fig. 8 Lift for solid disk.**

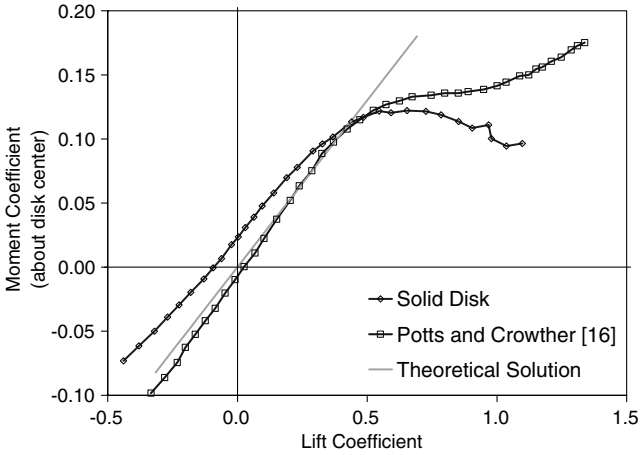


**Fig. 9 Pitching moment for solid disk.**

unexpected because differences in Reynolds numbers ($1 \times 10^6$ for the present data versus $3.78 \times 10^5$ for the Potts and Crowther data), wind-tunnel turbulence levels [26], and model edge treatments (beveled for the present data versus square for the Potts and Crowther data) can strongly affect the boundary-layer thickening and viscous effects that produce the moment break. Key parameters from the lift, drag, and moment curves are presented in Tables 4–6 for each of the models.

Figures 10 and 11 show lift and pitching moment data for the cutout disk in comparison to the vortex-lattice model results and the solid disk results. Both the lift and moment curve slopes show good agreement with the vortex-lattice analysis. However, as with the solid disk pitching moment results, there are noticeable offsets of both the lift and moment curves. The cutout disk is symmetric except for a 5 mm chamfer cut around the circumference of the outside and inside of the disk. Consequently, the lift and pitching moment at a zero angle of attack should both be quite small. Interference from the model support and shape of the leading edge [27] is the most likely explanation for the offset. In addition to this offset, the lift curve for the cutout disk also shows a marked increase in the lift curve slope starting at around 3–4 deg and continuing to about 10 deg. This increase is substantially greater than the increase seen in the solid disk lift curve. It appears that the flow through the cutout region affects the vortex lift resulting from separated flow off of the sharp edges of the disk. Interestingly, the pitching moment curve in Fig. 11 does not show nonlinearity in the same angle-of-attack region. Above 10 deg, the lift curve levels out and the maximum lift coefficient seen on the cutout disk is just over 1.0.

The drag for the solid and cutout disks is presented in Fig. 12 and compared with similar data from Potts and Crowther [16]. The minimum drag coefficients for the solid disk matches the data from Potts and Crowther fairly well (0.022 versus 0.018). The minimum drag coefficient for the cutout disk is twice that of the solid disk (0.022 versus 0.044, respectively). Because the reference area of the cutout disk is one-half that of the solid disk, the total dimensional drag of the cutout disk is equivalent to the drag of the solid disk in spite of having one-half the wetted area. Part of this increase in the drag coefficient can be explained by the difference in Reynolds number. As will be discussed later in the paper, it appears the boundary layer was primarily turbulent over the surface of the disks. For a turbulent boundary layer, the skin friction coefficient is approximately proportional to the Reynolds number to the −0.2 power [28] and, thus, proportional to the chord length to the −0.2 power. Because the difference in mean chord length between the cutout disk and the solid disk is a factor of 2, the difference in friction coefficient due to Reynolds number effects accounts for only approximately 15% of the increase in drag coefficient. The remaining difference may be interference drag related to the cutout opening. It is interesting to note that the cutout disk exhibits substantially lower drag at higher lift coefficients compared to the solid disk. This appears to be related to the increase in lift seen in Fig. 10, rather than a decrease in drag. When the drag data of Fig. 12 are replotted versus angle of attack instead of lift coefficient, the drag reduction is no longer apparent.

Figure 13 shows the lift behavior of the two Geobat models, one with a transition strip of grit on the leading edges and one without the transition strip. The lift curve for the solid and cutout disks are also shown for comparison. At low angles of attack, the lift characteristics for the Geobat models are very similar to the cutout disks. However, at higher angles of attack, there are significant differences. The nonlinear increase in lift coefficient noted for the cutout disk is not apparent for the Geobat models. Also, the cutout disk lift curve levels

**Table 4 Lift characteristics**

| | Geobat w/o strip | Geobat w/ strip | Cutout disk | Solid disk | Potts and Crowther [16] | Vortex-lattice cutout disk | Vortex-lattice solid disk |
|---|---|---|---|---|---|---|---|
| $\alpha_{L=0}$, deg | −3.14 | −3.03 | −2.27 | 0.07 | −0.79 | 0 | 0 |
| $C_{L_\alpha}$ [a] | 3.29 | 3.19 | 4.01 | 2.25 | 2.40 | 3.06 | 1.79 |
| $C_{L_\alpha}$ [b] | 4.07 | 4.91 | 1.37 | 3.20 | 2.48 | 3.06 | 1.79 |
| $C_{L,\max}$ | 1.32 | 1.41 | 1.09 | >1.10 | >1.34 | —— | —— |
| $\alpha_{\text{Stall}}$, deg | 18 | 19 | 16 | >22 | >30 | —— | —— |
| $C_{L,\alpha=0\ \text{deg}}$ | 0.191 | 0.212 | 0.143 | −0.002 | 0.026 | 0 | 0 |

[a]Estimated lift curve slope from −5 to 10 deg angle of attack.
[b]Estimated lift curve slope from 10 deg to $\alpha_{\text{Stall}}$ angle of attack.

**Table 5 Drag characteristics**

| | Geobat w/o strip | Geobat w/ strip | Cutout disk | Solid disk | Potts and Crowther [16] |
|---|---|---|---|---|---|
| $C_{D,0}$ | 0.043 | 0.046 | 0.044 | 0.022 | 0.018 |
| $\alpha_{\text{min drag}}$, deg | −2 | −1 | −2 | −2 | 0 |
| $L/D_{\max}$ | 7.97 | 7.65 | 4.96 | 4.36 | 7.45 |
| $\alpha_{L/D_{\max}}$, deg | 8 | 9 | 6 | 7 | 5 |

**Table 6 Moment characteristics**

| | Geobat w/o strip | Geobat w/ strip | Cutout disk | Solid disk | Potts and Crowther [16] | Vortex-lattice cutout disk | Vortex-lattice solid disk |
|---|---|---|---|---|---|---|---|
| $C_{\text{Mac}}$ | 0.069 | 0.065 | 0.084 | 0.020 | −0.007 | 0.0 | 0.0 |
| $x_{\text{ac}}$, % | 25.5 | 28.7 | 28.0 | 26.0 | 21.8 | 25.1 | 24.0 |

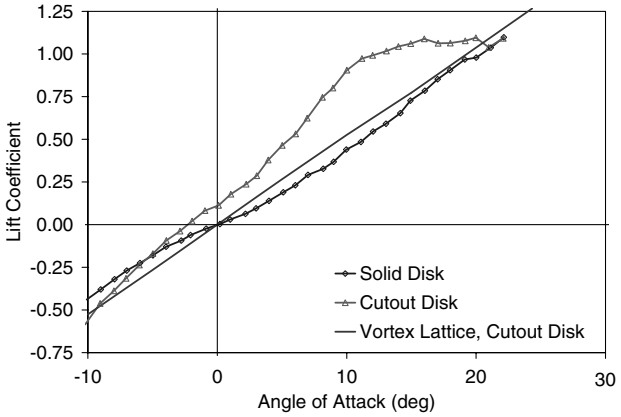


**Fig. 10 Lift for cutout disk.**

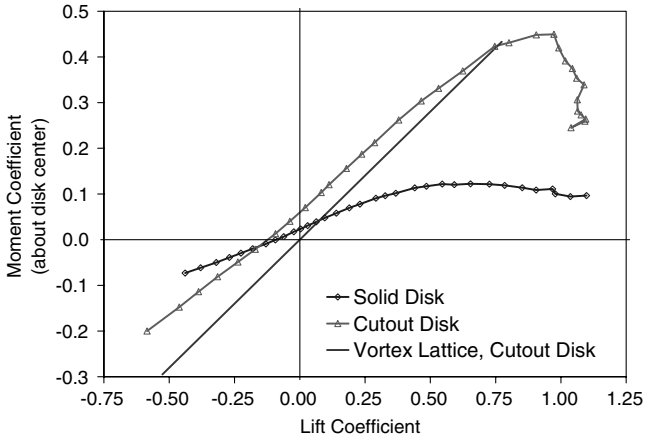


**Fig. 11 Pitching moment for cutout disk.**

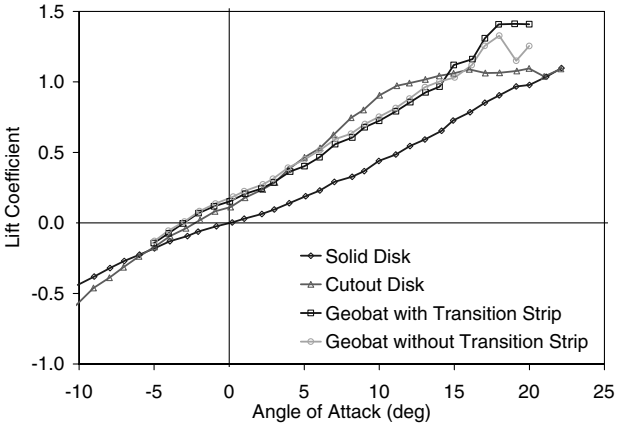


**Fig. 13 Lift for Geobat models.**

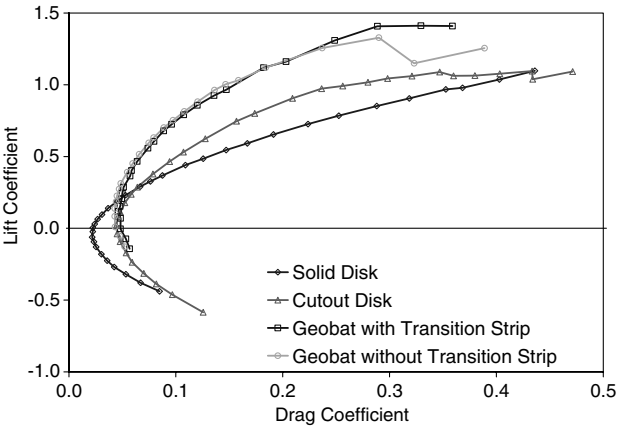


**Fig. 14 Drag for Geobat models.**

out above about 10 deg, whereas the Geobat curves continue to increase up to 18 or 19 deg. This suggests that the airfoil profile of the Geobat configuration delays the onset of separation versus the sharp leading edge of the cutout disk.

The measured drag of the Geobat models is shown in Fig. 14. The minimum drag for the Geobat models is virtually identical to that of the cutout disk. As lift increases, however, the drag of the Geobat model increases much more slowly than that of the cutout disk. When drag is plotted as a lift-to-drag ratio (shown in Fig. 15), the difference between the flat disks and the Geobat models is even more striking. The Geobat models exhibit lift-to-drag ratios of almost 8, whereas the cutout disk reaches just shy of 5. Some differences between the two Geobat models can be noticed in Fig. 15. The model without the transition strip exhibits a higher lift-to-drag ratio from approximately −3 to 16 deg. This is to be expected because the transition strip will tend to increase the turbulence of the boundary layer and thus increase the skin friction drag. At the highest angles of attack, the lift-to-drag ratio for the model without the transition strip drops down below that for the model with the transition strip. This suggests that the presence of the transition strip delays the onset of flow separation at these angles of attack, thus improving the lift-to-drag ratio. Overall, however, the differences between the two Geobat models is fairly slight. This suggests that either the transition strip is not effectively forcing the boundary layer to transition from laminar to turbulent or that there is little laminar flow to begin with. The Reynolds number for this test was just over 500,000, which is high enough that the transition strip should be highly effective; consequently, the data suggest that the extent of laminar flow over the Geobat model without the transition strip is small.

Figure 16 shows the pitching moment characteristics for the Geobat models and the two disk models. To allow comparison between the various planforms, the pitching moments for this figure

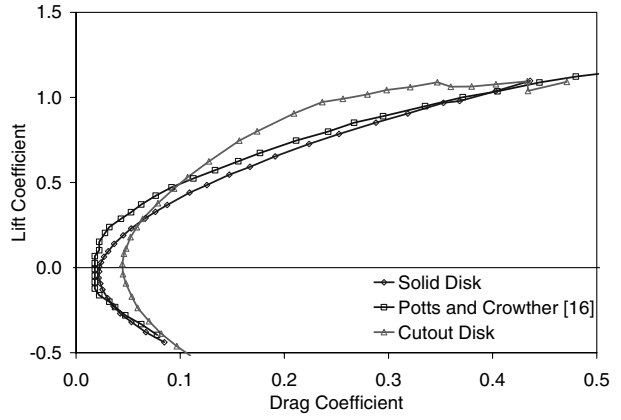


**Fig. 12 Drag polars for solid and cutout disks.**

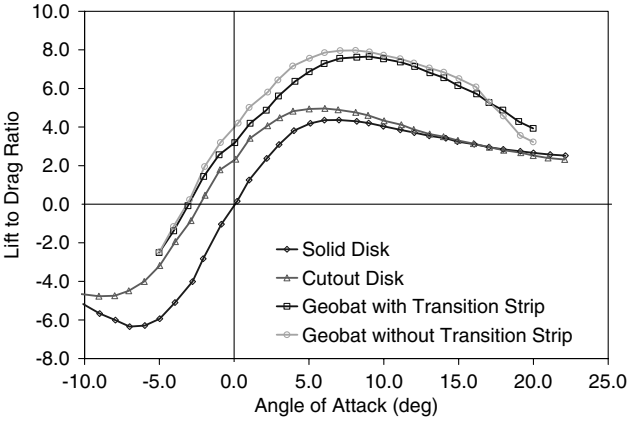


**Fig. 15 Lift-to-drag ratio for disks and Geobat models.**

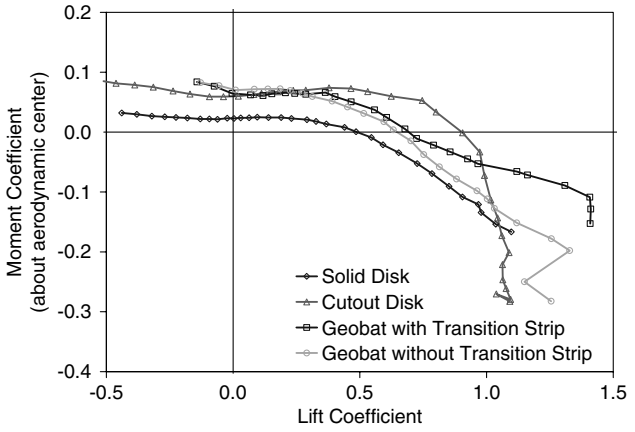


**Fig. 16 Pitching moment for Geobat models.**

were referenced to the aerodynamic centers of each of the planforms. Table 6 shows the estimated aerodynamic centers for each of the planforms. The aerodynamic centers were estimated by using a linear regression to find the slope of the pitching moment versus lift coefficient curve for each of the planforms in the low-angle-of-attack region. The vortex-lattice results indicate that the opening in the rear part of the cutout disk moves the aerodynamic center aft by about 1% of the disk diameter. The test data show a larger movement of 2% between the cutout disk and the solid disk. Averaging the aerodynamic centers of the Geobat models shows a movement of just over 1% behind the solid disk, which is consistent with the vortex-lattice result. In all cases, the change in aerodynamic center position is relatively small, with a maximum difference among the four models of 3.2%. Moreover, they are all just aft of the 25% chord position predicted by 2-D thin airfoil theory. This indicates that the longitudinal stability of the Geobat configuration should be similar to that of a disk, assuming the same c.g. position. The advantage of the Geobat configuration, then, is that by removing the material over the cutout area on the aft portion of the disk and assuming a uniform weight distribution over the disk, the c.g. is moved forward from the 50% chord position to the 42% chord position, thus requiring less weight shift forward to achieve a statically stable design.

The pitching moment for the Geobat models and the cutout disk are very close at low lift coefficients. The pitching moment for the solid disk is substantially lower. As mentioned earlier, it is probable that the low-angle-of-attack pitching moment is due to interference from the model support because the Geobat models and the cutout disk are roughly symmetric top to bottom. Interestingly, the behavior of the Geobat models and the solid disk are quite similar as lift coefficient increases and similar to the lenticular reentry vehicles studied in [10,11]. The moment break for these three models starts to occur around lift coefficients of 0.3–0.5, and they all drop off at roughly the same rate. The cutout disk behaves a little differently, maintaining a constant pitching moment up to a lift coefficient of approximately 0.7. It then drops off very quickly.

## Conclusions

The wind-tunnel tests presented in this paper explored the aerodynamic characteristics of the Geobat configuration. The tests indicate that the Geobat has several advantages over a disk-shaped wing. For example, the lift curve slope for the Geobat configuration is substantially higher than that of a solid disk, which allows the Geobat to generate higher lift coefficients at lower angles of attack. Although the zero-lift drag coefficient for the Geobat was higher than that of the solid disk, at operating lift coefficients the airfoil profile of the Geobat reduces the amount of separation over the surface and reduces the drag below that of the solid disk. Moreover, vortex-lattice analysis of the Geobat planform indicates that the lift distribution over the Geobat is elliptical and, thus, efficient from an induced drag standpoint.

One of the challenges for a disk-shaped wing is that the aerodynamic center is near the 25% chord point, but the center of volume of the shape is at the midchord point. Thus, substantial ballast would be required to move the c.g. forward to achieve longitudinal static stability. The Geobat shape improves this in two ways. The Geobat planform shifts the aerodynamic center slightly aft by 1–2% and, by removing substantial area from the rear portion of the disk, the center of volume of the shape moves forward by almost 10%. Moreover, the layout of the Geobat places most of the mass of the aircraft in the forward part of the disk, further reducing the need for ballast to move the center of gravity forward of the aerodynamic center. At high angles of attack, the test data show a strong negative (stable) break in the pitching moment at stall for the Geobat as well as the other models tested.

Based on the experimental data presented here, the Geobat configuration showed itself to be superior to the solid disk shape in all areas except for two. First, the solid disk had a substantially lower zero-lift drag coefficient, and second, the solid disk shape did not exhibit a stall at the angles of attack tested. However, these "advantages" of the solid disk shape are perhaps not particularly significant. The drag advantage of the solid disk is quickly lost as the angle of attack and the lift coefficient increase to a practical level. Moreover, even though the solid disk shape did not stall up to the angles tested, it is unlikely to have a higher maximum lift capability than the Geobat and the amount of drag generated at the high angles of attack at which the solid disk achieves maximum lift would make operation at those angles of attack infeasible.

## Acknowledgments

This work was funded through a grant from Geobat Flying Saucer Aviation, Inc., with Randy Pollard as the grant monitor. Appreciation and acknowledgement is extended to the Geobat designer, Jack Jones. The authors would like to thank Andy Weldon for his machine shop support.

## References

[1] Stilley, G. D., "Aerodynamic Analysis of the Self Sustained Flare," Naval Ammunition Depot RDTR 199, Crane, IN, 1972.
[2] Stilley, G. D., and Carstens, D. L., "Adaptation of Frisbee Flight Principle to Delivery of Special Ordnance," AIAA Paper 72-982, 1972.
[3] Turner, C. C., *Old Flying Days*, Arno Press, New York, 1972.
[4] Snyder, C. L., "Aircraft," U.S. Patent No. 1,855,695, April 1932.
[5] Higgins, G. H., "The Comparison of Well Known and New Wing Sections Tested in the Variable Density Wind Tunnel," NACA TN 219, 1925.
[6] Johnson, R. B., "Uniplane," U.S. Patent No. 1,887,411, Nov. 1932.
[7] Zimmerman, C. H., "Flying Pancake," U.S. Patent No. 2,108,093, Feb. 1938.
[8] Schoeni, A., and Ginter, S., *Chance Vought V-173 and XFU-1 Flying Pancakes*, Vol. 21, Naval Fighters Series, Steve Ginter Publishing, Simi Valley, CA, 1992.
[9] Oberto, R. J., "Environmental Control Systems Selection for Manned Space Vehicles," Flight Accessories Lab. Technical Rept. ASD-TR-61-240, Pt. 2, Vol. 2, Wright–Patterson Air Force Base, 1962.
[10] Ware, G. M., "Static Stability and Control Characteristics at Low-Subsonic Speeds of a Lenticular Reentry Configuration," NASA TM-X-431, 1960.
[11] Ware, G. M., "Investigation of the Low-Subsonic Aerodynamic Characteristics of a Model of a Modified Lenticular Reentry Configuration," NASA TM-X-756, 1962.
[12] Kissinger, C. D., "Circular Wing Aircraft," U.S. Patent No. 3,871,602, March 1975.
[13] Myers, G. F., "Flying Machine," U.S. Patent No. 1,523,994, 20 Jan. 1925.
[14] Mitchell, T. L., "The Aerodynamic Response of Airborne Discs," MS Thesis, Univ. of Nevada, Las Vegas, NV, 1999.
[15] Yasuda, K., "Flight and Aerodynamic Characteristics of a Flying Disk," *Journal of the Japan Society for Aeronautical and Space Sciences*, Vol. 47, No. 547, 1999, pp. 314–320.
[16] Potts, J. R., and Crowther, W. J., "Frisbee Aerodynamics," AIAA Paper 2002-3150, 2002.
[17] Ali, W., "Aerodynamics of Rotating Disc Wings," Undergraduate Report, School of Engineering, Univ. of Manchester, Manchester,

England, UK, April 1998.
[18] Jordan, P. F., "Exact Solutions for Lifting Surfaces," *AIAA Journal*, Vol. 11, No. 8, Aug. 1973, pp. 1123–1129. doi:10.2514/3.50557
[19] Tuck, E. O., and Lazauskas, L., "Lifting Surfaces with Circular Planforms," *Journal of Ship Research*, Vol. 49, 2005, pp. 274–278.
[20] Jones, J. M., "Three Wing Circular Planform Body," U.S. Patent No. 5,520,355, May 1996.
[21] Recktenwald, B. D., "Aerodynamic Testing of a Circular Planform Concept Aircraft," M.S. Thesis, Auburn Univ., Auburn, AL, 2008.
[22] Katz, J., and Plotkin, A., *Low-Speed Aerodynamics*, 2nd ed., Cambridge Univ. Press, New York, 2001.
[23] Drela, M., and Youngren, H., "Athena Vortex Lattice," Ver. 3.26, Massachusetts Inst. of Technology, Cambridge, MA, 29 April 2006.
[24] Anderson, J. D., *Fundamentals of Aerodynamics*, 4th ed., McGraw–Hill, New York, 2007.
[25] McCormick, B. W., *Aerodynamics, Aeronautics, and Flight Mechanics*, Wiley, New York, 1979.
[26] Böttcher, J., and Wedemeyer, E., "The Flow Downstream of Screens and Its Influence on the Flow in the Stagnation Region of Cylindrical Bodies," *Journal of Fluid Mechanics*, Vol. 204, 1989, pp. 501–522. doi:10.1017/S0022112089001850
[27] Bartlett, G. E., and Vidal, R. J., "Experimental Investigation of Influence of Edge Shape on the Aerodynamic Characteristics of Low Aspect Ratio Wings at Low Speeds," *Journal of the Aeronautical Sciences*, Vol. 22, No. 8, 1955, pp. 517–533.
[28] Anderson, J. D., *Introduction to Flight*, 6th ed., McGraw–Hill, New York, 2008.